ACS OMEGA

Open Access

http://pubs.acs.org/journal/acsodf

Article

Aromatic 2,2-Diphenylethylamine Ligand Exchange of $FA_{0.9}Cs_{0.1}PbBr_3$ Perovskite Nanocrystals for High-Efficiency Pure Green Light-Emitting Diodes

Shoki Mizoguchi, Shunsuke Sumikoshi, Haruka Abe, Yuta Ito, Ryohei Yamakado, and Takayuki Chiba*

Cite This: *ACS Omega* 2024, 9, 34692−34699

Read Online

ACCESS | Metrics & More | Article Recommendations | Supporting Information

ABSTRACT: Perovskite nanocrystals (NCs) with long alkyl ligands cannot easily form high-quality composite films owing to their poor dispersibility in π-conjugated small molecules and polymer host materials. In this study, we demonstrated that the aromatic ligand exchange of mixed-cation $FA_{0.9}Cs_{0.1}PbBr_3$ NCs using 2,2-diphenylethylamine (DPEA) can not only enable the fabrication of high-efficiency light-emitting diodes (LEDs) but also allows dispersibility in host materials. The DPEA-NC film exhibited a pure green wavelength of 530 nm and a full width at half-maximum of 20.9 nm with a photoluminescence quantum yield of 90.9%. A DPEA-NC LED achieved a luminance of 39,700 cd/m^2 and an external quantum efficiency of 18.6% even in a thick NC film. Interestingly, the DPEA-NCs formed a composite film with small-molecule tris(4-carbazoyl-9-ylphenyl)amine. The operational stability of this composite LED was eight times higher than that of the DPEA-NC LED owing to enhanced hole−electron charge balance and the suppression of perovskite NC degradation. Therefore, the aromatic DPEA ligand exchange of perovskite NCs is an effective way to improve their electrical properties and operational device stabilities.

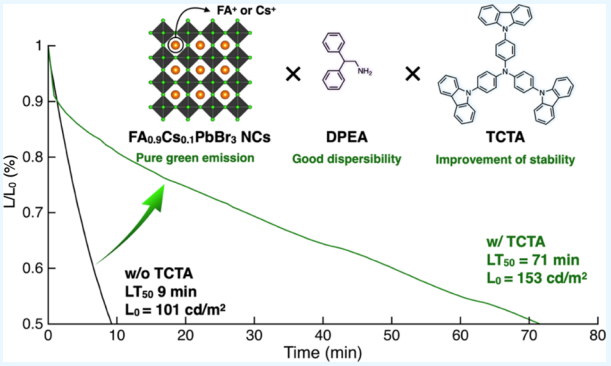

INTRODUCTION

Metal halide perovskite nanocrystals (NCs) with the chemical formula ABX_3, (A = methylammonium ion (MA^+), formamidinium ion (FA^+), Cs^+; B = Pb^{2+}, Sn^{2+}; and X = Cl^-, Br^-, I^-), are expected to be used for light-emitting diode (LED) applications owing to their high color purity and narrow emission spectrum that has a full width at half-maximum (fwhm) below 30 nm in the ultraviolet−visible−near-infrared (UV−vis−NIR) region.[1−6] The emission color of perovskite NCs can be controlled by tuning the halide composition[7,8] and particle size.[9,10] Cs-based $CsPb(Cl/Br)_3$ and $CsPb(Br/I)_3$ NC LEDs have achieved both BT.2020 blue and red color ranges,[2,11] whereas the $CsPbBr_3$ NC LEDs have not achieved the BT.2020 green color range.[12] A-site mixed-cation $FA_{1-x}Cs_xPbBr_3$ NCs overcome this limitation and have exhibited the ability to tune their band gap and photoluminescence (PL) peak wavelength precisely.[13] A-site composition engineering with mixed cations effectively suppresses halide-ion migration, thus improving the operational device lifetime of perovskite NC LEDs.[14]

The surface ligands of perovskite NCs capped with long alkyl chains play an important role in controlling the particle size during the synthesis and in achieving high colloidal stability in nonpolar solvents. However, long alkyl ligands, such as oleic acid and oleylamine, are generally insulating and hence reduce the electrical conductivity of the perovskite NC films. In other words, the charge carrier injection and transport properties are deteriorated, resulting in a higher driving voltage of the NC LEDs as the thickness of the perovskite NC film increases.[15,16] Therefore, several methods for the ligand exchange of perovskite NCs have been developed, incorporating postsynthetic treatment with short alkyl ligands,[17,18] quaternary ammonium salts,[16,19] zwitterionic ligands,[20] multiamine ligands,[21] inorganic ligands,[3,22] and aromatic ligands.[23−26] Thus, far, perovskite NC LEDs have exhibited a poor operational device lifetime that is shorter than several hundred hours[27,28] owing to strong exciton−charge carrier interactions[29,30] and ion migration in NC films.[31] To overcome these disadvantages, a composite film was developed with chemically stable host materials, such as polymer binders[32,33] and metal−organic frameworks.[34,35] This film was reported to improve the chemical, thermal, and water stabilities of perovskite NCs; however, perovskite NC:small-molecule composite LEDs have not been achieved. Furthermore, perovskite NCs with long alkyl ligands have poor dispersibility

Received: April 11, 2024
Revised: July 7, 2024
Accepted: July 10, 2024
Published: August 1, 2024

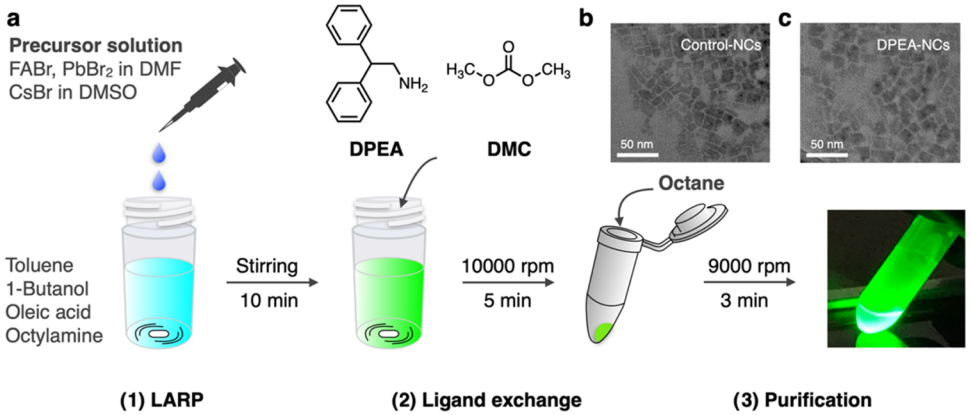

Figure 1. (a) Synthesis, ligand exchange, and purification procedures of mixed-cation $FA_{1-x}Cs_xPbBr_3$ NCs. TEM images of (b) control-NCs and (c) DPEA-NCs.

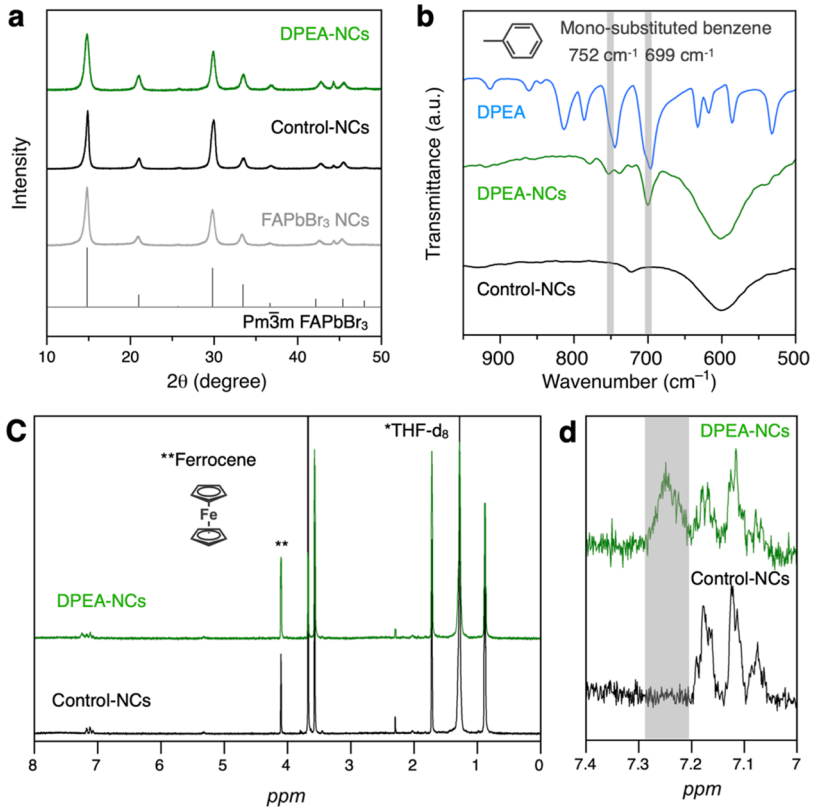

Figure 2. Characterization of the crystal structure and surface composition. (a) XRD patterns of $FAPbBr_3$−NCs, control-NCs, and DPEA-NCs. (b) FTIR spectra of DPEA, control-NCs, and DPEA-NCs. (c, d) ^{1}H NMR spectra of the control-NCs and DPEA-NCs (*THF-d8, **ferrocene as an internal standard).

when π-conjugated small molecules or polymers are used as host materials, making the formation of high-quality composite films difficult.

In this study, we demonstrated that the aromatic 2,2-diphenylethylamine (DPEA) ligand exchange of mixed-cation $FA_{0.9}Cs_{0.1}PbBr_3$ NCs can be used to simultaneously achieve pure green emission with a high photoluminescence quantum yield (PLQY) and dispersibility in host materials. Mixed-cation $FA_{0.9}Cs_{0.1}PbBr_3$ NCs were synthesized via ligand-assisted reprecipitation (LARP), and aromatic DPEA ligand exchange was performed during the purification process. The DPEA-NC film exhibited a high PLQY (90.9%) and pure green emission with a peak wavelength of 530 nm. The DPEA ligand exchange did not affect the crystal structure and particle size before ligand exchange NCs. The fabricated DPEA-NC LEDs exhibited a luminance of 39700 cd/m^2 and an external quantum yield (EQE) of 18.6% even in a thick NC film. In addition, the DPEA-NCs improve dispersibility in the aromatic solvent and a small-molecule host material, tris(4-carbazoyl-9-ylphenyl)amine (TCTA). The DPEA-NC:TCTA composite LED achieved a higher efficiency and operational device stability than the DPEA-NC LED owing to an enhanced hole−electron charge balance and the suppression of perovskite NC degradation.

https://doi.org/10.1021/acsomega.4c03488
ACS Omega 2024, 9, 34692−34699

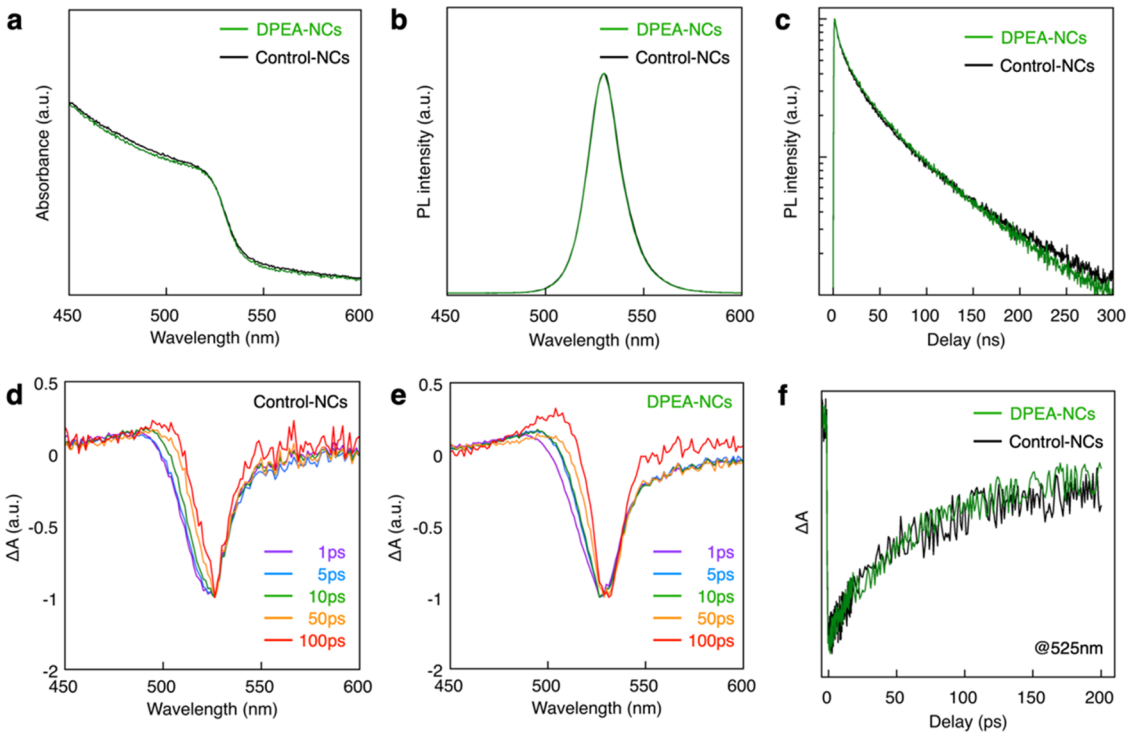

Figure 3. Characterization of optical properties. (a) UV−vis absorption spectra. (b) PL spectra. (c) PL decay lifetimes of the control-NC and DPEA-NCs films. Femtosecond transient absorption of (d) the control-NC film and (e) DPEA-NC film. (f) Transient absorption bleach recovery kinetics of the control-NC and DPEA-NC films measured at 525 nm.

RESULTS AND DISCUSSION

A-site mixed-cation $FA_{1-x}Cs_xPbBr_3$ NCs (x = 0, 0.1, and 0.4) were synthesized via the one-step LARP method by using *N*,*N*-dimethylformamide (DMF) or dimethyl sulfoxide (DMSO) as a precursor solvent, in which metal halides have a high solubility (Figure S1; details are presented in the Experimental Methods section). The mixed-cation ratio of FA/Cs was altered by changing the ratio of formamidine hydrobromide (FABr) to cesium bromide (CsBr). The incorporation of 10% Cs^+ into $FAPbBr_3$ improved their optical properties. The crystal structures, chemical compositions, and optical properties of $FAPbBr_3$ and $FA_{0.9}Cs_{0.1}PbBr_3$ NCs are shown in Figures S2−S4.

Postsynthetic ligand exchange of the $FA_{0.9}Cs_{0.1}PbBr_3$ NCs (control-NCs) was performed to produce a composite film with small-molecule host materials using aromatic DPEA in the purification process (Figure 1a). The type of antisolvent used in the reprecipitation purification process is crucial because of ligand desorption from the perovskite NC surface, which results in a low PLQY owing to the formation of surface defects or perovskite NC aggregation.[15] Moreover, perovskite NCs with low ligand density have poor redispersibility in nonpolar solvents. Conventional antisolvents, such as butyl acetate (ε = 5.01), ethyl acetate (ε = 6.02), methyl acetate (ε = 6.68), diglyme (ε = 7.23), and butanol (ε = 17.1), could not reprecipitate, whereas dimethyl carbonate (DMC) (ε = 3.10) could be adequately reprecipitated (Figure S5). DPEA was dissolved in low-dielectric-constant DMC and was then added into the $FA_{0.9}Cs_{0.1}PbBr_3$ NC octane dispersion, followed by stirring for 5 min; the dispersion was centrifugated to collect DPEA-$FA_{0.9}Cs_{0.1}PbBr_3$ NCs (details are presented in the Experimental Methods section). Transmission electron microscopy (TEM) images of the control-NCs and DPEA-NCs are shown in Figure 1b,c, respectively. The estimated average size was approximately 15−16 nm for both (Figure S6).

To investigate the crystal structure of the DPEA-NCs, X-ray diffraction (XRD) was performed. Diffraction peaks attributed to the $Pm\bar{3}m$ $FAPbBr_3$ phase were observed for the control-NCs and DPEA-NCs, indicating that the DPEA ligand exchange treatment does not influence their crystal structures (Figure 2a).[36] X-ray photoelectron spectroscopy (XPS) was performed to determine the chemical composition of the perovskite NCs before and after DPEA treatment (Figure S7). The Cs 3d and Br 3d core peaks of the DPEA-NCs clearly shift to lower binding energy levels compared with those of the control-NCs. We investigated the surface ligand composition by using Fourier transform infrared (FTIR) spectroscopy (Figure 2b). C−H bending vibration peaks of the benzene ring at 752 and 699 cm^{-2} were observed for the DPEA-NCs. A proton nuclear magnetic resonance (^{1}H NMR) analysis was performed to estimate the detailed surface compositions of the control-NCs and DPEA-NCs using ferrocene as an internal standard (Figure 2c,d). Phenyl resonance in the range of 7.2−7.3 ppm was clearly observed for the DPEA-NCs, in agreement with the FTIR results. The integrated ratios of alkene/ferrocene were 0.11 and 0.047 for the control-NCs and DPEA-NCs, respectively, suggesting that the DPEA ligand exchange treatment results in oleic acid desorption. Conversely, the phenyl/ferrocene resonance of the DPEA-NCs of 0.11 was twice that of oleic acid.

The optical properties, i.e., the UV−vis absorption and PL spectra, of the control-NCs and DPEA-NCs are shown in Figure 3a,b, respectively. The DPEA-NC film exhibited UV−vis absorption and PL spectra identical to those of the control-NC film; the optical band gap, PL peak, and fwhm were 2.39 eV, 530, and 20.9 nm, respectively. The DPEA-NC film

https://doi.org/10.1021/acsomega.4c03488
ACS Omega 2024, 9, 34692−34699

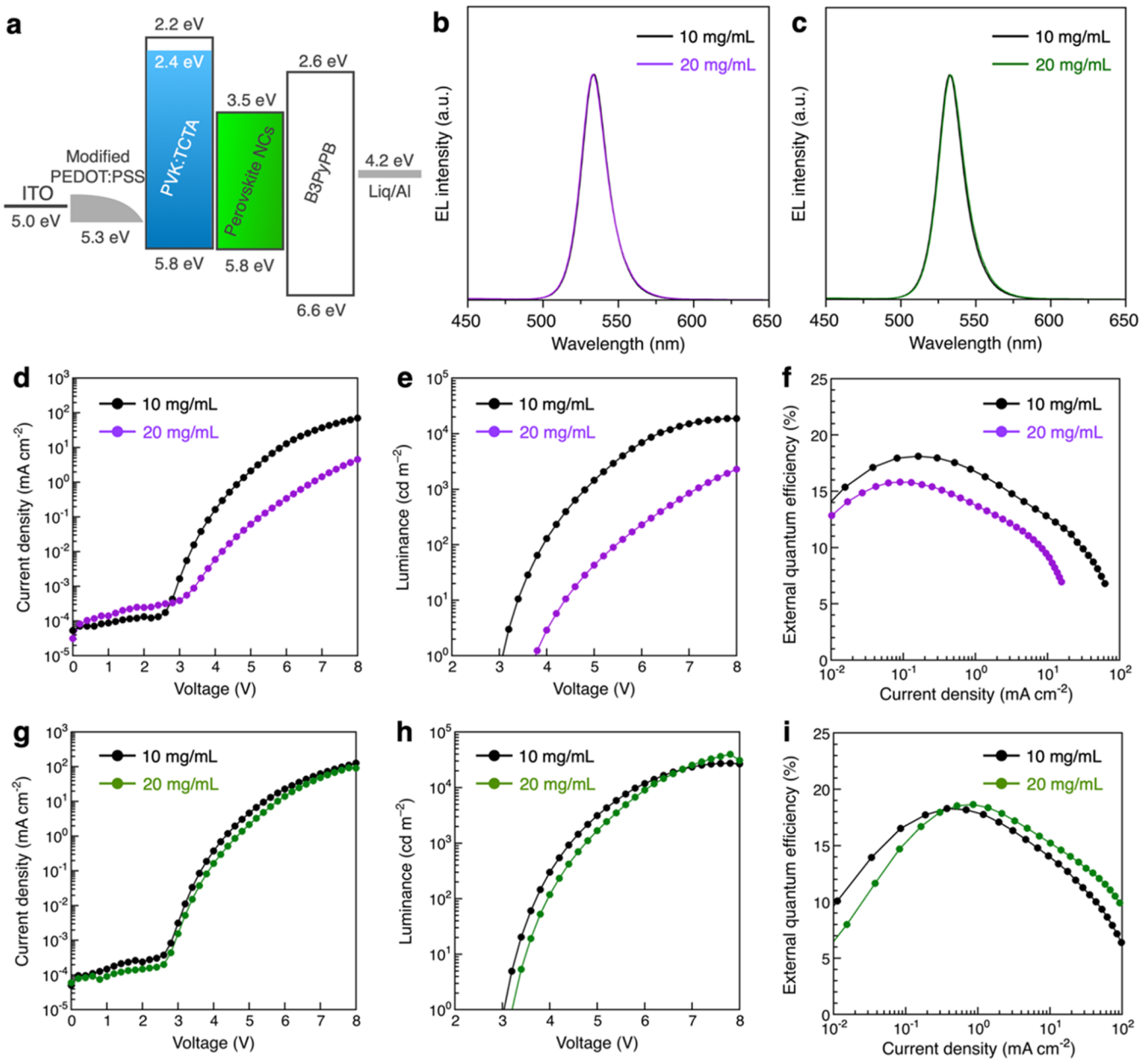

Figure 4. Device characterization of control-NC and DPEA-NC LEDs with different ink concentrations: 10 and 20 mg/mL. (a) Energy diagram of the LEDs. EL spectra of the (b) control-NC LED and (c) DPEA-NC LED. Current density, luminance, and EQE of the (d–f) control-NC LED and (g–i) DPEA-NC LED.

exhibited a PLQY (90.9%) similar to that of the control-NC film (88.2%), which had a value comparable to that of the dispersion state. Conversely, the twice-washed control-NCs without DPEA treatment exhibited a lower PLQY of 53.8%, owing to the formation of surface defects. Thus, the postsynthetic DPEA ligand exchange treatment effectively passivated surface defects during multiple purification processes. The transient PL decay times were 64.3 and 60.6 ns for the control- and DPEA-NC films, respectively (Figure 3c), which agrees well with the previously reported values for the control-NC film.[5,37] Femtosecond transient absorption of the control and DPEA-NC films was performed to investigate the photoexcited carrier dynamics. The DPEA-NC film exhibits similar bleaching peak and recovery kinetics to the control-NC film in Figure 3d–f, indicating that postsynthetic DPEA ligand exchange does not influence the recombination and transition dynamics of $FA_{0.9}Cs_{0.1}PbBr_3$ NCs.

To verify the perovskite NC film thickness before and after DPEA ligand exchange, LEDs based on the control-NC and DPEA-NCs using different ink concentrations (10–20 mg/mL) were fabricated: indium tin oxide (ITO) (130 nm)/poly(3,4-ethylenedioxythiophene)/poly(styrene-sulfonate) (PEDOT:PSS) with Nafion (40 nm)/PVK: 30 wt % TCTA (20 nm)/$FA_{0.9}Cs_{0.1}PbBr_3$ NCs (10 or 20 mg/mL)/1,3-bis(3,5-dipyrid-3-ylphenyl)benzene (B3PyPB) (40 nm)/lithium 8-quinolate (Liq) (1 nm)/Al (100 nm). To improve the hole injection and transport properties of PVK, the small-molecule host material TCTA was doped into PVK and used as a hole-transport layer. The thicknesses of the $FA_{0.9}Cs_{0.1}PbBr_3$ NCs films were 15 nm for an ink concentration of 10 mg/mL and 30 nm for an ink concentration of 20 mg/mL. The energy

https://doi.org/10.1021/acsomega.4c03488
ACS Omega 2024, 9, 34692–34699

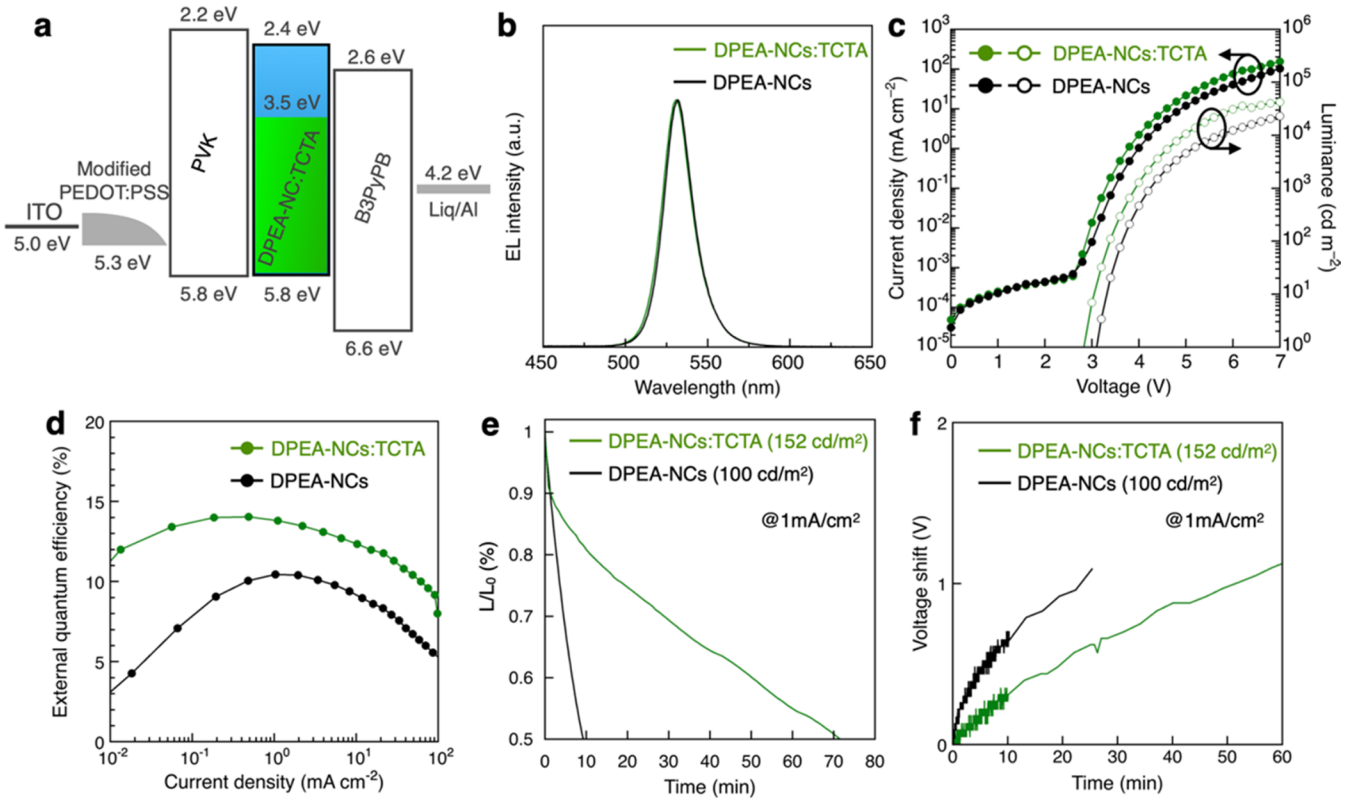

Figure 5. Device characterization of the DPEA-NC LEDs with the small-molecule host material TCTA. (a) Energy diagram of the LEDs. (b) EL spectra with high color purity (inset: CIE coordinates of the green color range for LEDs), (c) current density−voltage− luminance, (d) EQE−current density, (e) operational device lifetime, and (f) voltage shift at a constant current density of 1 mA cm^{-2}.

diagram of the LEDs is shown in Figure 4a. The valence band and conduction band of the DPEA-NCs were estimated at 5.84 and 3.54 eV, respectively, via ultraviolet photoelectron spectroscopy (UPS) and the optical band gap (Figure S8). The DPEA-NC LED exhibited a similar electroluminescence (EL) peak of 533 nm and an fwhm of 21.3 nm to the control-NC LED, regardless of the $FA_{0.9}Cs_{0.1}PbBr_3$ NC film thickness (Figure 4b,c). Strong film-thickness dependence was observed for the control-NC LEDs, with the thicker control-NC film exhibiting a higher turn-on voltage and lower current density and luminance as shown in Figure 4d,e. The external quantum efficiency (EQE) of the control-NC LED decreased from 18.1% (20 mg/mL) to 15.8% (10 mg/mL) with an increase in the NC thickness, owing to the insulating property of the long alkyl ligand-based control-NC film (Figures 4f and S9). In contrast, the DPEA-NC LEDs exhibited a similar driving voltage, luminance, and EQE regardless of the NC film thickness (Figure 4g−i and Table S1). The peak luminance and EQE of the DPEA-NC LEDs were 27300 cd/m^2 and 18.3%, respectively, for the thin NC film (10 mg/mL) and 39700 cd/m^2 and 18.6%, respectively, for the thick NC film (20 mg/mL), indicating that the aromatic ligand-based DPEA-NCs are useful for a wide range of thicknesses owing to the improved charge-transport properties compared with the long alkyl ligand-based control-NC film. The DPEA-NC LEDs exhibited an operational device lifetime (LT_{50}) of 25 min (initial luminance of 100 cd/m^2 at a current density of 1 mA/cm^2; Figure S10).

We also demonstrated the dispersion of the DPEA-NCs into small-molecule host material TCTA to improve hole injection from the hole-transport layer for a lower driving voltage and longer operational device lifetime. Figure S11 shows photographs of the control-NC:TCTA and DPEA-NC:TCTA films and dispersions. The control-NC:TCTA film exhibited a poor film morphology and aggregation in the dispersion state, whereas the DPEA-NC:TCTA film exhibited good film formability and clear dispersion without NC aggregation because the aromatic DPEA ligand was highly compatible in the π-conjugated small-molecule structure. The DPEA-NC:TCTA composite film exhibited a similar UV−vis absorption spectrum, PL spectrum, and PL decay lifetime to the DPEA-NC film; thus, the use of TCTA as a host material in perovskite NCs does not affect the optical properties (Figure S12 and Table S2). The DPEA-NC:TCTA LEDs were fabricated by using the following device structure: ITO (130 nm)/PEDOT:PSS with Nafion (40 nm)/PVK (20 nm)/DPEA-NC:TCTA/B3PyPB (40 nm)/Liq (1 nm)/Al (100 nm), as shown in Figure 5a. The DPEA-NC:TCTA LED exhibited a pure green EL peak of 530 nm and an fwhm of 21.2 nm, corresponding to the CIE coordinates (0.177, 0.769), which are close to the BT.2020 green color range (Figure 5b). The DPEA-NC:TCTA LED exhibited a lower turn-on voltage (2.84 V) and higher luminance (43,800 cd/m^2) than the DPEA-NC LED without TCTA (3.10 V and 32,200 cd/m^2) (Figure 5c). The DPEA-NC:TCTA LED exhibited a higher EQE (14.0%) than the DPEA-NC LED (10.4%; Figure 5d and Table S3). Moreover, the use of TCTA as a host material allowed a high EQE to be maintained in the high current density range, owing to the improvement of the hole−electron charge balance. The operational device lifetime and voltage shift of the LEDs were obtained at 1 mA/cm^2, corresponding to an initial luminance of 100−150 cd/m^2 (Figure 5e). The

https://doi.org/10.1021/acsomega.4c03488
ACS Omega 2024, 9, 34692−34699

DPEA-NC:TCTA LED exhibited a longer LT_{50} (71 min) than that of the control-NC LED (9 min). In addition, a large voltage shift was observed for the control-NC LED, which was suppressed for the composite LEDs (Figure 5f). Therefore, the use of hole-transport TCTA as a host material is effective for not only enhancing the hole injection and transport properties but also improving their operational device stability (Table S4).

The DPEA-NC:polymer composite film was also found to enhance the water stability. Ionic perovskite NCs are highly sensitive to moisture, resulting in a phase transition to an optically inactive state. Therefore, the chemically stable polymer poly(methyl methacrylate) (PMMA) was used as a binder for the NCs owing to its high solubility in toluene. A water stability test was performed on the polymer composite films (Figure S13). For the control-NCs, control-NC:PMMA, and DPEA-NCs, the luminance completely disappeared after 1 h of storage in water, whereas DPEA-NC:PMMA maintained luminance even after 1 week of storage in water; therefore, aromatic DPEA plays a role in the compatibility with PMMA. These results suggested that the use of a composite film can significantly improve water stability, which can be useful for downconversion color filter applications.

CONCLUSIONS

In conclusion, postsynthetic aromatic DPEA-NCs exhibited enhanced electrical properties and dispersibility in the small-molecule host material TCTA. The PLQYs of $FA_{0.9}Cs_{0.1}PbBr_3$ films were 88.2% for control-NCs, 90.9% for DPEA-NCs, and 93.2% for DPEA-NC:TCTA with pure green emission. The control-NC LED exhibited a higher driving voltage and lower EQE for a thick layer, whereas a DPEA-NC LED could be operated with a thick layer while maintaining a high EQE of 18.6%. In addition, the DPEA-NC:TCTA composite-film-based LED exhibited increased device efficiency and operational lifetime because the degradation of $FA_{0.9}Cs_{0.1}PbBr_3$ NCs was suppressed. The use of aromatic DPEA ligand and small-molecule host composites is effective for enhancing the electrical and device properties.

EXPERIMENTAL METHODS

Materials. FABr (99.99%), DPEA (98.0%), DMC (98.0%), and DMSO (99.0%) were purchased from the Tokyo Chemical Industry. Lead bromide(II) ($PbBr_2$, 99.999%), cesium bromide (CsBr, 99.999%), DMF (anhydrous 99.8%), oleic acid (90%), and *n*-octylamine (99%) were purchased from Sigma-Aldrich. Toluene (dehydrated super, 99.5%) was purchased from KANTO CHEMICAL, and *n*-butyl alcohol (99.0%) and *n*-octane (98.0%) were purchased from Wako.

For the fabrication of the LEDs, a PEDOT:PSS (AI4083) was purchased from Clevious. Nafion perfluorinated resin (aqueous dispersion, 10 wt % in H_2O) and PVK (25,000−50,000) were purchased from Sigma-Aldrich. 1,3-Bis(3,5-dipyrid-3-ylphenyl)benzene (B3PyPB) was purchased from FLASK Co., Ltd. TCTA and Liq were purchased from e-Ray Optoelectronics Technology. All chemicals were used as received.

Synthesis of $FAPbBr_3$ NCs. To prepare a precursor solution, FABr (12.5 mg, 0.10 mmol) and $PbBr_2$ (73.4 mg, 0.20 mmol) were dissolved in anhydrous DMF (0.30 mL). Thereafter, the precursor solution (0.15 mL) was added to anhydrous toluene (5.0 mL), 1-butanol (2.0 mL), oleic acid (0.30 mL), and octylamine (0.030 mL), followed by stirring for 10 min at room temperature. The resulting NC mixture was centrifuged at 10000 rpm for 5 min, and the precipitate was collected. The precipitate was then redispersed in *n*-octane or toluene and filtered (PTFE filter) before use.

Synthesis of $Cs_xFA_{1-x}PbBr_3$ NCs. CsBr (50 mg, 0.24 mmol) was added to anhydrous DMSO (1.0 mL) and stirred overnight at 70 °C in a N_2-filled glovebox to achieve complete dissolution. Subsequently, the precursor solutions of FABr and $PbBr_2$ dissolved in DMF and CsBr dissolved in DMSO were mixed in the same manner as for the precursor solution of the $FAPbBr_3$ NCs described above. At this time, the amounts of the A-site compounds, i.e., FABr and CsBr, were adjusted so that the total amount of FABr and CsBr was 0.1 mmol. The other synthesis and purification processes were identical to those of the $FAPbBr_3$ NCs.

Ligand Exchange of DPEA. DPEA (0.05 and 0.2 mmol) was dissolved in DMC (1.0 mL). Thereafter, an equal volume of DMC solution with DPEA was added to the synthesized $Cs_xFA_{1-x}PbBr_3$ NCs, and the supernatant was removed via centrifugation at 9000 rpm for 3 min. The precipitate was redispersed in *n*-octane or toluene and centrifuged again at 9000 rpm for 3 min. The supernatant was filtered (PTFE filter) before use.

Characterization. XRD patterns were acquired by using a Rigaku SmartLab diffractometer. NMR spectra were obtained using a JEOL 400 spectrometer operated at a ^1H frequency of 500 MHz, and FTIR spectra were measured by using a HORIBA IRAffinity-1S instrument. TEM was performed by using a JEOL JEM-2100F instrument. UV−vis absorption and PL spectra were measured by using a Shimadzu UV-3150 UV−vis−NIR spectrophotometer and a HORIBA FluoroMax Plus luminescence spectrometer, respectively. The PLQY was measured by using a Hamamatsu C9920−01 integral sphere system. XPS and UPS were conducted using a Thermo Fisher Scientific Theta probe with a He I UV source (21.22 eV) under a high vacuum of $\sim 10^{-6}$ Pa and an operating voltage maintained at −6 V. SEM was performed by using a JEOL JSM-6700F system operated at 20 kV. The surface roughness was measured using a Bruker Dimension Icon atomic force microscope (AFM) system in the tapping mode. Transient absorption spectra were obtained via the pump−probe method (Helios, Ultrafast). The output of a Ti/sapphire laser system (Mai Tai, Spectra Physics) was split into two paths (800 nm, 100 fs, and 1 kHz). One of these was frequency-doubled as a pump beam, and the other was converted into a white light continuum as a probe beam. They were focused on a sample, and the spectrum of the probe beam was recorded as a function of the delay time between the pump and the probe beam.

Fabrication of NC LEDs. ITO substrates were cleaned by using deionized water via ultrasonic spin cleaning and then through UV−ozone treatment for 10 min. Thereafter, the PEDOT:PSS blend with Nafion (40 nm thick) was spin-coated (2000 rpm/30 s) onto the ITO substrate, followed by annealing at 150 °C for 10 min. PVK (8 mg/mL in chlorobenzene) or PVK:30 wt % TCTA (7:3 v/v) was spin-coated onto PEDOT:PSS with a Nafion layer, followed by annealing at 150 °C for 30 min. The NCs (10 mg/mL in Octane) or an NC blend with a 25−30 wt % host material was spin-coated onto the PVK or PVK: 30 wt % TCTA. Finally, B3PyPB (40 nm), Liq (1 nm), and Al (100 nm) were sequentially deposited via thermal evaporation. The fabricated

https://doi.org/10.1021/acsomega.4c03488
ACS Omega 2024, 9, 34692−34699

LEDs with an active area of 4 mm^2 were encapsulated using epoxy glue and glass covers in a N_2-filled glovebox. The EL spectra were acquired by using a Hamamatsu PMA-11 photonic multichannel analyzer. The current density versus voltage and luminance versus voltage characteristics were recorded using a Keithley source unit 2400 and a Minolta CS2000 system.

PMMA Dispersion Film. DPEA ligand-exchanged $Cs_xFA_{1-x}PbBr_3$ NCs (10 mg/mL in toluene) were mixed with PMMA (30 mg/mL in toluene) at a volume ratio of 5:95 (v/v). The films were then spin-coated at 500 rpm for 30 s.

■ ASSOCIATED CONTENT

Supporting Information

The Supporting Information is available free of charge at https://pubs.acs.org/doi/10.1021/acsomega.4c03488.

XRD; XPS; UV−vis; PL; PL decay; UPS; operational device stability; and water stability test (PDF)

■ AUTHOR INFORMATION

Corresponding Author

Takayuki Chiba − *Graduate School of Organic Materials Science, Yamagata University, Yonezawa, Yamagata 992-8510, Japan;* orcid.org/0000-0002-6893-7874; Phone: +81-238-26-3595; Email: T-chiba@yz.yamagata-u.ac.jp

Authors

Shoki Mizoguchi − *Graduate School of Organic Materials Science, Yamagata University, Yonezawa, Yamagata 992-8510, Japan*

Shunsuke Sumikoshi − *Graduate School of Organic Materials Science, Yamagata University, Yonezawa, Yamagata 992-8510, Japan*

Haruka Abe − *Graduate School of Organic Materials Science, Yamagata University, Yonezawa, Yamagata 992-8510, Japan*

Yuta Ito − *Graduate School of Organic Materials Science, Yamagata University, Yonezawa, Yamagata 992-8510, Japan*

Ryohei Yamakado − *Graduate School of Organic Materials Science, Yamagata University, Yonezawa, Yamagata 992-8510, Japan;* orcid.org/0000-0003-4085-9226

Complete contact information is available at: https://pubs.acs.org/10.1021/acsomega.4c03488

Notes

The authors declare no competing financial interest.

■ ACKNOWLEDGMENTS

T.C. acknowledges the Extensive Support for Young Promising Researchers from the New Energy and Industrial Technology Development Organization (NEDO), the Strategic International Collaborative Research Program (JPMJSC2111), and the START Program (ST211002QB) of the Japan Science and Technology Agency (JST).

■ REFERENCES

(1) Protesescu, L.; Yakunin, S.; Bodnarchuk, M. I.; Krieg, F.; Caputo, R.; Hendon, C. H.; Yang, R. X.; Walsh, A.; Kovalenko, M. V. Nanocrystals of Cesium Lead Halide Perovskites (CsPbX(3), X = Cl, Br, and I): Novel Optoelectronic Materials Showing Bright Emission with Wide Color Gamut. *Nano Lett.* **2015**, *15*, 3692−3696.

(2) Chiba, T.; Hayashi, Y.; Ebe, H.; Hoshi, K.; Sato, J.; Sato, S.; Pu, Y. J.; Ohisa, S.; Kido, J. Anion-exchange red perovskite quantum dots with ammonium iodine salts for highly efficient light-emitting devices. *Nat. Photonics* **2018**, *12*, 681−687.

(3) Dong, Y.; Wang, Y. K.; Yuan, F.; Johnston, A.; Liu, Y.; Ma, D.; Choi, M. J.; Chen, B.; Chekini, M.; Baek, S. W.; Sagar, L. K.; Fan, J.; Hou, Y.; Wu, M.; Lee, S.; Sun, B.; Hoogland, S.; Quintero-Bermudez, R.; Ebe, H.; Todorovic, P.; Dinic, F.; Li, P.; Kung, H. T.; Saidaminov, M. I.; Kumacheva, E.; Spiecker, E.; Liao, L. S.; Voznyy, O.; Lu, Z. H.; Sargent, E. H. Bipolar-shell resurfacing for blue LEDs based on strongly confined perovskite quantum dots. *Nat. Nanotechnol.* **2020**, *15*, 668−674.

(4) Hassan, Y.; Park, J. H.; Crawford, M. L.; Sadhanala, A.; Lee, J.; Sadighian, J. C.; Mosconi, E.; Shivanna, R.; Radicchi, E.; Jeong, M.; Yang, C.; Choi, H.; Park, S. H.; Song, M. H.; De Angelis, F.; Wong, C. Y.; Friend, R. H.; Lee, B. R.; Snaith, H. J. Ligand-engineered bandgap stability in mixed-halide perovskite LEDs. *Nature* **2021**, *591*, 72−77.

(5) Kim, Y. H.; Kim, S.; Kakekhani, A.; Park, J.; Park, J.; Lee, Y. H.; Xu, H. X.; Nagane, S.; Wexler, R. B.; Kim, D. H.; Jo, S. H.; Martinez-Sarti, L.; Tan, P.; Sadhanala, A.; Park, G. S.; Kim, Y. W.; Hu, B.; Bolink, H. J.; Yoo, S.; Friend, R. H.; Rappe, A. M.; Lee, T. W. Comprehensive defect suppression in perovskite nanocrystals for high-efficiency light-emitting diodes. *Nat. Photonics* **2021**, *15*, 148−155.

(6) Bi, C.; Yao, Z.; Sun, X.; Wei, X.; Wang, J.; Tian, J. Perovskite Quantum Dots with Ultralow Trap Density by Acid Etching-Driven Ligand Exchange for High Luminance and Stable Pure-Blue Light-Emitting Diodes. *Adv. Mater.* **2021**, *33*, No. 2006722.

(7) Nedelcu, G.; Protesescu, L.; Yakunin, S.; Bodnarchuk, M. I.; Grotevent, M. J.; Kovalenko, M. V. Fast Anion-Exchange in Highly Luminescent Nanocrystals of Cesium Lead Halide Perovskites (CsPbX3, X = Cl, Br, I). *Nano Lett.* **2015**, *15*, 5635−5640.

(8) Akkerman, Q. A.; D'Innocenzo, V.; Accornero, S.; Scarpellini, A.; Petrozza, A.; Prato, M.; Manna, L. Tuning the Optical Properties of Cesium Lead Halide Perovskite Nanocrystals by Anion Exchange Reactions. *J. Am. Chem. Soc.* **2015**, *137*, 10276−10281.

(9) Levchuk, I.; Osvet, A.; Tang, X.; Brandl, M.; Perea, J. D.; Hoegl, F.; Matt, G. J.; Hock, R.; Batentschuk, M.; Brabec, C. J. Brightly Luminescent and Color-Tunable Formamidinium Lead Halide Perovskite FAPbX(3) (X = Cl, Br, I) Colloidal Nanocrystals. *Nano Lett.* **2017**, *17*, 2765−2770.

(10) Dong, Y.; Qiao, T.; Kim, D.; Parobek, D.; Rossi, D.; Son, D. H. Precise Control of Quantum Confinement in Cesium Lead Halide Perovskite Quantum Dots via Thermodynamic Equilibrium. *Nano Lett.* **2018**, *18*, 3716−3722.

(11) Chevalier, O. J. G. L.; Nakamuro, T.; Sato, W.; Miyashita, S.; Chiba, T.; Kido, J.; Shang, R.; Nakamura, E. Precision Synthesis and Atomistic Analysis of Deep-Blue Cubic Quantum Dots Made via Self-Organization. *J. Am. Chem. Soc.* **2022**, *144*, 21146−21156.

(12) Yuan, S.; Wang, Z. K.; Zhuo, M. P.; Tian, Q. S.; Jin, Y.; Liao, L. S. Self-Assembled High Quality CsPbBr(3) Quantum Dot Films toward Highly Efficient Light-Emitting Diodes. *ACS Nano* **2018**, *12*, 9541−9548.

(13) Liang, F. C.; Jhuang, F. C.; Fang, Y. H.; Benas, J. S.; Chen, W. C.; Yan, Z. L.; Lin, W. C.; Su, C. J.; Sato, Y.; Chiba, T.; Kido, J.; Kuo, C. C. Synergistic Effect of Cation Composition Engineering of Hybrid Cs(1-x) FA(x) PbBr(3) Nanocrystals for Self-Healing Electronics Application. *Adv. Mater.* **2023**, *35*, No. 2207617.

(14) Li, N.; Song, L.; Jia, Y.; Dong, Y.; Xie, F.; Wang, L.; Tao, S.; Zhao, N. Stabilizing Perovskite Light-Emitting Diodes by Incorporation of Binary Alkali Cations. *Adv. Mater.* **2020**, *32*, No. 1907786.

(15) Hoshi, K.; Chiba, T.; Sato, J.; Hayashi, Y.; Takahashi, Y.; Ebe, H.; Ohisa, S.; Kido, J. Purification of Perovskite Quantum Dots Using Low-Dielectric-Constant Washing Solvent "Diglyme" for Highly Efficient Light-Emitting Devices. *ACS Appl. Mater. Interfaces* **2018**, *10*, 24607−24612.

(16) Chiba, T.; Hoshi, K.; Pu, Y. J.; Takeda, Y.; Hayashi, Y.; Ohisa, S.; Kawata, S.; Kido, J. High-Efficiency Perovskite Quantum-Dot Light-Emitting Devices by Effective Washing Process and Interfacial Energy Level Alignment. *ACS Appl. Mater. Interfaces* **2017**, *9*, 18054−18060.
(17) Koscher, B. A.; Swabeck, J. K.; Bronstein, N. D.; Alivisatos, A. P. Essentially Trap-Free CsPbBr(3) Colloidal Nanocrystals by Postsynthetic Thiocyanate Surface Treatment. *J. Am. Chem. Soc.* **2017**, *139*, 6566−6569.
(18) Wu, L.; Zhong, Q.; Yang, D.; Chen, M.; Hu, H.; Pan, Q.; Liu, H.; Cao, M.; Xu, Y.; Sun, B.; Zhang, Q. Improving the Stability and Size Tunability of Cesium Lead Halide Perovskite Nanocrystals Using Trioctylphosphine Oxide as the Capping Ligand. *Langmuir* **2017**, *33*, 12689−12696.
(19) Pan, J.; Quan, L. N.; Zhao, Y.; Peng, W.; Murali, B.; Sarmah, S. P.; Yuan, M.; Sinatra, L.; Alyami, N. M.; Liu, J.; Yassitepe, E.; Yang, Z.; Voznyy, O.; Comin, R.; Hedhili, M. N.; Mohammed, O. F.; Lu, Z. H.; Kim, D. H.; Sargent, E. H.; Bakr, O. M. Highly Efficient Perovskite-Quantum-Dot Light-Emitting Diodes by Surface Engineering. *Adv. Mater.* **2016**, *28*, 8718−8725.
(20) Krieg, F.; Ochsenbein, S. T.; Yakunin, S.; Ten Brinck, S.; Aellen, P.; Suess, A.; Clerc, B.; Guggisberg, D.; Nazarenko, O.; Shynkarenko, Y.; Kumar, S.; Shih, C. J.; Infante, I.; Kovalenko, M. V. Colloidal CsPbX(3) (X = Cl, Br, I) Nanocrystals 2.0: Zwitterionic Capping Ligands for Improved Durability and Stability. *ACS Energy Lett.* **2018**, *3*, 641−646.
(21) Zeng, Q.; Zhang, X.; Bing, Q.; Xiong, Y.; Yang, F.; Liu, H.; Liu, J.-y.; Zhang, H.; Zheng, W.; Rogach, A. L.; Yang, B. Surface Stabilization of Colloidal Perovskite Nanocrystals via Multi-amine Chelating Ligands. *ACS Energy Lett.* **2022**, *7*, 1963−1970.
(22) Song, J.; Fang, T.; Li, J.; Xu, L.; Zhang, F.; Han, B.; Shan, Q.; Zeng, H. Organic-Inorganic Hybrid Passivation Enables Perovskite QLEDs with an EQE of 16.48. *Adv. Mater.* **2018**, *30*, No. 1805409.
(23) Dai, J.; Xi, J.; Li, L.; Zhao, J.; Shi, Y.; Zhang, W.; Ran, C.; Jiao, B.; Hou, X.; Duan, X.; Wu, Z. Charge Transport between Coupling Colloidal Perovskite Quantum Dots Assisted by Functional Conjugated Ligands. *Angew. Chem., Int. Ed.* **2018**, *57*, 5754−5758.
(24) Zhang, L.; Zhang, Q.; Xing, X.; Jiang, Y.; He, T.; Huang, Y.; Ma, Z.; Yang, J.; Yuan, M. Conjugated Alkylamine by Two-Step Surface Ligand Engineering in CsPbBr3 Perovskite Nanocrystals for Efficient Light-Emitting Diodes. *ChemNanoMat* **2019**, *5*, 318−322.
(25) Pan, J.; Shang, Y.; Yin, J.; De Bastiani, M.; Peng, W.; Dursun, I.; Sinatra, L.; El-Zohry, A. M.; Hedhili, M. N.; Emwas, A. H.; Mohammed, O. F.; Ning, Z.; Bakr, O. M. Bidentate Ligand-Passivated CsPbI(3) Perovskite Nanocrystals for Stable Near-Unity Photoluminescence Quantum Yield and Efficient Red Light-Emitting Diodes. *J. Am. Chem. Soc.* **2018**, *140*, 562−565.
(26) Zhao, H.; Chen, H.; Bai, S.; Kuang, C.; Luo, X.; Teng, P.; Yin, C.; Zeng, P.; Hou, L.; Yang, Y.; Duan, L.; Gao, F.; Liu, M. High-Brightness Perovskite Light-Emitting Diodes Based on FAPbBr3 Nanocrystals with Rationally Designed Aromatic Ligands. *ACS Energy Lett.* **2021**, *6*, 2395−2403.
(27) Liu, Y.; Dong, Y.; Zhu, T.; Ma, D.; Proppe, A.; Chen, B.; Zheng, C.; Hou, Y.; Lee, S.; Sun, B.; Jung, E. H.; Yuan, F.; Wang, Y. K.; Sagar, L. K.; Hoogland, S.; de Arquer, F. P. G.; Choi, M. J.; Singh, K.; Kelley, S. O.; Voznyy, O.; Lu, Z. H.; Sargent, E. H. Bright and Stable Light-Emitting Diodes Based on Perovskite Quantum Dots in Perovskite Matrix. *J. Am. Chem. Soc.* **2021**, *143*, 15606−15615.
(28) Li, H.; Lin, H.; Ouyang, D.; Yao, C.; Li, C.; Sun, J.; Song, Y.; Wang, Y.; Yan, Y.; Wang, Y.; Dong, Q.; Choy, W. C. H. Efficient and Stable Red Perovskite Light-Emitting Diodes with Operational Stability > 300 h. *Adv. Mater.* **2021**, *33*, No. 2008820.
(29) Ye, F.; Shan, Q.; Zeng, H.; Choy, W. C. H. Operational and Spectral Stability of Perovskite Light-Emitting Diodes. *ACS Energy Lett.* **2021**, *6*, 3114−3131.
(30) Jiang, Y.; Cui, M.; Li, S.; Sun, C.; Huang, Y.; Wei, J.; Zhang, L.; Lv, M.; Qin, C.; Liu, Y.; Yuan, M. Reducing the impact of Auger recombination in quasi-2D perovskite light-emitting diodes. *Nat. Commun.* **2021**, *12*, No. 336.
(31) Han, B.; Yuan, S.; Cai, B.; Song, J.; Liu, W.; Zhang, F.; Fang, T.; Wei, C.; Zeng, H. Green Perovskite Light-Emitting Diodes with 200 h Stability and 16% Efficiency: Cross-Linking Strategy and Mechanism. *Adv. Funct. Mater.* **2021**, *31*, No. 2011003, DOI: 10.1002/adfm.202011003.
(32) Raja, S. N.; Bekenstein, Y.; Koc, M. A.; Fischer, S.; Zhang, D.; Lin, L.; Ritchie, R. O.; Yang, P.; Alivisatos, A. P. Encapsulation of Perovskite Nanocrystals into Macroscale Polymer Matrices: Enhanced Stability and Polarization. *ACS Appl. Mater. Interfaces* **2016**, *8*, 35523−35533.
(33) Jiang, G.; Guhrenz, C.; Kirch, A.; Sonntag, L.; Bauer, C.; Fan, X.; Wang, J.; Reineke, S.; Gaponik, N.; Eychmuller, A. Highly Luminescent and Water-Resistant CsPbBr(3)-CsPb(2)Br(5) Perovskite Nanocrystals Coordinated with Partially Hydrolyzed Poly(methyl methacrylate) and Polyethylenimine. *ACS Nano* **2019**, *13*, 10386−10396.
(34) Chen, Z.; Gu, Z. G.; Fu, W. Q.; Wang, F.; Zhang, J. A Confined Fabrication of Perovskite Quantum Dots in Oriented MOF Thin Film. *ACS Appl. Mater. Interfaces* **2016**, *8*, 28737−28742.
(35) Tsai, H.; Shrestha, S.; Vilá, R. A.; Huang, W.; Liu, C.; Hou, C.-H.; Huang, H.-H.; Wen, X.; Li, M.; Wiederrecht, G.; Cui, Y.; Cotlet, M.; Zhang, X.; Ma, X.; Nie, W. Bright and stable light-emitting diodes made with perovskite nanocrystals stabilized in metal−organic frameworks. *Nat. Photonics* **2021**, *15*, 843−849.
(36) Zhumekenov, A. A.; Saidaminov, M. I.; Haque, M. A.; Alarousu, E.; Sarmah, S. P.; Murali, B.; Dursun, I.; Miao, X. H.; Abdelhady, A. L.; Wu, T.; Mohammed, O. F.; Bakr, O. M. Formamidinium Lead Halide Perovskite Crystals with Unprecedented Long Carrier Dynamics and Diffusion Length. *ACS Energy Lett.* **2016**, *1*, 32−37.
(37) Zu, Y.; Xi, J.; Li, L.; Dai, J.; Wang, S.; Yun, F.; Jiao, B.; Dong, H.; Hou, X.; Wu, Z. High-Brightness and Color-Tunable FAPbBr(3) Perovskite Nanocrystals 2.0 Enable Ultrapure Green Luminescence for Achieving Recommendation 2020 Displays. *ACS Appl. Mater. Interfaces* **2020**, *12*, 2835−2841.

https://doi.org/10.1021/acsomega.4c03488
ACS Omega 2024, 9, 34692−34699